mathematics

Article

A Novel Spacetime Boundary-Type Meshless Method for Estimating Aquifer Hydraulic Properties Using Pumping Tests

Cheng-Yu Ku [1] and Chih-Yu Liu [2,*]

[1] School of Engineering, National Taiwan Ocean University, Keelung 202301, Taiwan; chkst26@mail.ntou.edu.tw
[2] Department of Civil Engineering, National Central University, Taoyuan 320317, Taiwan
* Correspondence: liu20452003@ncu.edu.tw

Abstract: This article introduces a new boundary-type meshless method designed for solving axisymmetric transient groundwater flow problems, specifically for aquifer tests and estimating hydraulic properties. The method approximates solutions for axisymmetric transient groundwater flow using basis functions that satisfy the governing equation by solving the inverse boundary value problem in the spacetime domain. The effectiveness of this method was demonstrated through validation with the Theis solution, which involves transient flow to a well in an infinite confined aquifer. The study included numerical examples that predicted drawdown at various radial distances and times near pumping wells. Additionally, an iterative scheme, namely, the fictitious time integration method, was employed to iteratively determine the hydraulic properties during the pumping test. The results indicate that this approach yielded highly accurate solutions without relying on the conventional time-marching scheme. Due to its temporal and spatial discretization within the spacetime domain, this method was found to be advantageous for estimating crucial hydraulic properties, such as the transmissivity and storativity of an aquifer.

Keywords: meshless; spacetime; pumping; hydraulic property; groundwater; aquifer

MSC: 76S05; 65N35

check for updates

Citation: Ku, C.-Y.; Liu, C.-Y. A Novel Spacetime Boundary-Type Meshless Method for Estimating Aquifer Hydraulic Properties Using Pumping Tests. *Mathematics* **2023**, *11*, 4497. https://doi.org/10.3390/math11214497

Academic Editors: Wenzhen Qu and Yan Gu

Received: 29 September 2023
Revised: 27 October 2023
Accepted: 29 October 2023
Published: 31 October 2023

1. Introduction

Due to climate change, the occurrence of extreme climate events, such as drought, is often found around the world such that groundwater usage is increased dramatically [1–3]. Groundwater is typically extracted for human use by withdrawing water from pumping wells located in drilled boreholes within the aquifer. The groundwater flow to an extraction well is axisymmetric [4–6], which refers to flow that is symmetric with respect to a central axis. Axisymmetric conditions are therefore suitable for modeling the aquifer tests because the impact of stresses on the groundwater system is radially symmetric [7–9]. The Theis solution has commonly been applied to analyze problems involving transient flow to a well, which assumes radial flow to a well of constant discharge in an infinite aquifer [10,11]. Axisymmetric flow in a pumping well can be simulated using numerical methods, such as an axisymmetric finite-difference flow model. This model is specifically designed to analyze pumping tests in a heterogeneous aquifer [12–14]. Although mesh-generation techniques can be employed to solve axisymmetric flow problems, they necessitate the use of extremely dense meshes to achieve satisfactory accuracy [15,16]. Meshfree methods were found to be highly promising as competitive alternatives due to their simplicity in characterization and flexibility in solving inverse problems through boundary collocation points, resulting in reduced computational complexity [17–19].

Meshfree methods offer significant benefits for problems involving complex and irregular geometry, as they do not rely on mesh construction. The Trefftz method, the method of fundamental solutions, and the radial basis function collocation method have gained widespread popularity and are commonly employed [12–14]. Meshfree methods can be classified into boundary-type and domain-type meshless methods. This classification is based on whether the basis functions satisfy the governing equation or not. The boundary-type meshless method is particularly advantageous for solving axisymmetric flow problems because it solely relies on boundary and source collocation points, eliminating the need for an extensive mesh [20–23]. Meanwhile, meshless approaches using the Minkowski spacetime were recently proposed. The Minkowski spacetime domain combines an n-dimensional Euclidean space with a one-dimensional time dimension, creating an $n + 1$-dimensional manifold specifically for solving transient flow problems [24]. Within this spacetime domain, spacetime basis functions are essential for discretizing both spatial and temporal aspects of the governing equation. Additionally, this domain facilitates the transformation of boundary and initial data into spacetime data. This allows for the direct application of initial and boundary data on spacetime boundary collocation points. The original axisymmetric flow problems, which are initially or finally defined in n dimensions, can be reformulated as inverse boundary value problems in $n + 1$ dimensions [24]. The use of the time-marching technique is therefore unnecessary in this spacetime approach. Recently, these spacetime meshless methods have found extensive use in the field of hydrogeology, encompassing applications such as modeling saturated and unsaturated flow problems, addressing interactions with surface water, and tackling shallow water wave problems [25–28].

This article introduces a novel spacetime boundary-type meshless method designed for the resolution of axisymmetric transient groundwater flow problems. The fundamental features of this method are rooted in the spacetime domain, facilitating the direct application of initial and boundary data onto spacetime boundary collocation points. The core of this approach involves approximating solutions for axisymmetric transient groundwater flow through the utilization of basis functions that satisfy the governing equation. This is achieved by addressing the inverse boundary value problem within the spacetime domain. The robustness and reliability of the proposed method were validated through a series of comprehensive assessments. These included comparisons with established solutions, such as the Theis solution and exact solutions. Furthermore, a set of numerical examples was meticulously examined. These examples encompassed a range of scenarios, including the prediction of drawdown near pumping wells. These scenarios involved instances such as pumping in an infinite confined aquifer, addressing axisymmetric transient groundwater flow problems, and simulating radial flow toward multiple wells within a confined aquifer system. The organizational structure of this research article is as follows: In Section 2, the mathematical foundations of the proposed spacetime boundary-type meshless method are delineated, providing a clear framework for understanding the approach's formulation. Section 3 provides numerical examples that predict drawdown at different radial distances and times in the vicinity of pumping wells. In Section 4, we present several applications demonstrating the estimation of aquifer hydraulic properties through pumping tests. Finally, Section 5 offers a summary of the study's main findings and conclusions.

2. Methodology

2.1. Governing Equation for Radial Flow

In a confined aquifer, the piezometric surface refers to the groundwater surface elevation observed in a well that is drilled into and screened within the confined aquifer, where the groundwater level exceeds the upper confining layer (refer to Figure 1). The flow toward a pumping well in a confined aquifer is described using the following equation:

$$\frac{\partial^2 h}{\partial r^2} + \frac{1}{r}\frac{\partial h}{\partial r} = \frac{S}{T}\frac{\partial h}{\partial t}, \tag{1}$$

where h is the total head, r is the radial distance measured from the centerline of the well, S is the storativity, T denotes the transmissivity, and t denotes the time. Equation (1) represents the mass conservation of the groundwater flow in the radial direction, considering variations in storage volume due to the expansion or contraction of confined water caused by pressure changes. For the pumping rate, denoted as Q, in the boundary condition equation below, a negative sign is applied, resulting in a negative direction in the radial coordinate (r) while pumping. The initial condition, external boundary condition, and internal boundary condition are respectively described as

$$h(r,\ t = 0) = 0, \tag{2}$$

$$h(r = \infty, t) = 0, \tag{3}$$

$$\lim_{r=r_w}(2\pi r T\frac{\partial h}{\partial r}) = -Q. \tag{4}$$

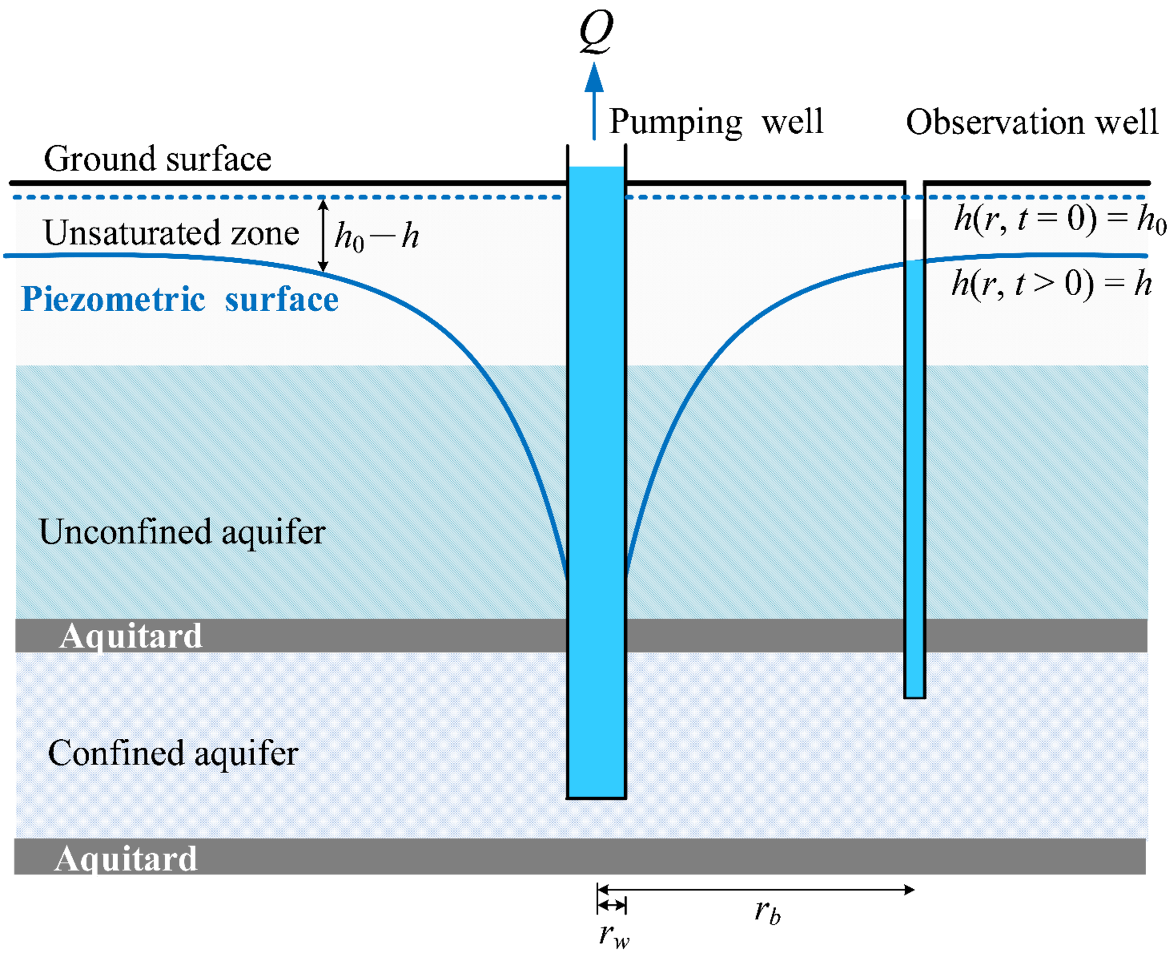

Figure 1. Illustrations of transient groundwater flow to a pumping well in a confined aquifer.

This well facilitates a constant flow rate initiated at $t = 0$. The solution for the associated simplified partial differential equation, as represented by Equation (1), was established by Theis in 1935 [29]. The resulting solution, known as the Theis solution, is described as

$$h = h_0(x, y) - \frac{Q}{4\pi T}W(u), \tag{5}$$

where $h_0(x, y)$ denotes the solution of the steady-state flow general solution, Q denotes the discharge of the pumping well, $W(u)$ denotes the well function, and u denotes a dimensionless parameter defined as $u = r^2S/4T(t - t_0)$. The well function is approximated using a truncated series expansion as follows:

$$W(u) = E_1(u) = -\gamma - \ln u + u - \frac{u^2}{2(2!)} + \frac{u^3}{3(3!)} - \frac{u^4}{4(4!)} + \ldots, \tag{6}$$

where $E_1(u)$ denotes the exponential integral and γ denotes Euler's constant, which is defined as 0.5772157 [11,29]. The equation of the Theis solution relates the drawdown to the hydraulic conductivity of the aquifer, transmissivity, pumping rate, radial distance from the well, and time since the pumping started, as defined in Equation (5). The Theis solution is based on the assumption of radial flow toward a well with constant discharge in an infinite aquifer. It was developed by Charles Theis in 1935 and is widely used in hydrogeology for analyzing well tests and estimating aquifer properties [29,30]. The Theis solution is based on the assumptions of radial symmetry, homogeneity, and infinite extent of the aquifer. It provides a mathematical expression for the drawdown, which is the decrease in the groundwater level caused by pumping at a given distance from the well.

2.2. Basis Function for the Axisymmetric Transient Groundwater Flow Problems

To derive time-dependent solutions for the axisymmetric diffusion equation, we utilize a technique known as the method of variable separation [24]. An initial assumption is made for the solution, which is as follows:

$$h(r,t) = R(r)T(t). \tag{7}$$

To simplify matters, we examine the following equation:

$$R' = \frac{dR(r)}{dr},\ R'' = \frac{d^2R(r)}{dr^2},\ \text{and } T' = \frac{dT(t)}{dt}. \tag{8}$$

By incorporating the equations mentioned above into Equation (1), we can derive

$$\alpha^2(R''T + \frac{1}{r}R'T + \frac{1}{r^2}RT) = RT', \tag{9}$$

where α^2 denotes T/S. When we divide both sides of the equation above by $R(r)T(t)$, we can express Equation (9) as the following set of equations:

$$\frac{R''}{R} + \frac{1}{r}\frac{R'}{R} - \frac{1}{\alpha^2}\frac{T'}{T} = 0, \tag{10}$$

$$\frac{1}{\alpha^2}\frac{T'}{T} = \lambda, \tag{11}$$

where λ denotes a constant. To ascertain the eigenvalue of the aforementioned equations, we introduce a constant parameter to ensure that the resulting value is either negative or positive. Detailed formulations are outlined below.

(1) The first case: $\lambda = 0$

Considering the first case, $\lambda = 0$, the governing equation becomes

$$R'' + \frac{1}{r}R' = 0. \tag{12}$$

The following solutions are obtained as

$$\begin{matrix} R = C_1 \ln r + C_2 \\ T = C_3 \end{matrix}, \tag{13}$$

where C_1, C_2, and C_3 represent constants. Inserting Equation (13) into Equation (1), we may obtain

$$h(r,t) = \overline{C}_1 \ln r + \overline{C}_2, \tag{14}$$

where $\overline{C}_1$ and $\overline{C}_2$ are constant.

(2) The second case: $\lambda = k^2$

Considering the second case, $\lambda = k^2$, the governing equation becomes

$$r^2 R'' + rR' - r^2 k^2 R = 0, \tag{15}$$

We derive the solutions as follows:

$$\begin{array}{l} R = C_4 I_0(kr) + C_5 K_0(kr) \\ T = C_6 e^{\alpha^2 k^2 t} \end{array}, \tag{16}$$

where I_0 denotes the modified Bessel function of the first kind; K_0 denotes the modified Bessel function of the second kind; and C_4, C_5, and C_6 are constants. Substituting Equation (16) into Equation (1), we have

$$h(r,t) = \overline{C}_3 e^{\alpha^2 k^2 t} I_0(kr) + \overline{C}_4 e^{\alpha^2 k^2 t} K_0(kr), \tag{17}$$

where $\overline{C}_3$ and $\overline{C}_4$ are constants.

(3) The third case: $\lambda = -k^2$

Considering the third case, $\lambda = -k^2$, the governing equation becomes

$$r^2 R'' + rR' + r^2 k^2 R = 0. \tag{18}$$

We obtain the solutions as follows:

$$\begin{array}{l} R = C_7 J_0(kr) + C_8 Y_0(kr) \\ T = C_9 e^{-\alpha^2 k^2 t} \end{array}, \tag{19}$$

where C_7, C_8, and C_9 are constants, and J_0 and Y_0 denote the Bessel functions of the first and second kind, respectively. By substituting Equation (19) into Equation (1), we arrive at the following expression:

$$h(r,t) = \overline{C}_5 e^{-\alpha^2 k^2 t} J_0(kr) + \overline{C}_6 e^{-\alpha^2 k^2 t} Y_0(kr), \tag{20}$$

where $\overline{C}_5$ and $\overline{C}_6$ are constants.

Combining all the solutions derived from the previously mentioned formulations, we can express the linearly independent solutions of the axisymmetric diffusion equation, as given by Equation (1), as follows:

$$h(r,t) \approx \overline{C}_1 \ln r + \overline{C}_2 + \sum_{k=1}^{w} [\overline{C}_3 e^{\alpha^2 k^2 t} I_0(kr) + \overline{C}_4 e^{\alpha^2 k^2 t} K_0(kr) + \overline{C}_5 e^{-\alpha^2 k^2 t} J_0(kr) + \overline{C}_6 e^{-\alpha^2 k^2 t} Y_0(kr)], \tag{21}$$

where w represents the order of the basis functions used for approximating the solution. In the case of an infinite domain, consideration is limited to negative basis functions. Consequently, the simplification of the above equation can be expressed as follows:

$$h(r,t) \approx \overline{C}_1 \ln r + \sum_{k=1}^{w} \overline{a}_k e^{\alpha^2 k^2 t} I_0(kr). \tag{22}$$

Using the final time and boundary conditions, we can discretize Equation (22) at various boundary collocation points along the spacetime boundary. This process leads to the formation of a system of linear equations, as shown in the following equation:

$$\mathbf{AC} = \mathbf{B}, \tag{23}$$

where $\mathbf{A} = \begin{bmatrix} 1 & e^{\alpha^2 t_1} I_0(r_1) & e^{-\alpha^2 t_1} J_0(r_1) & \cdots & e^{-\alpha^2 w^2 t_1} J_0(r_1) \\ 1 & e^{\alpha^2 t_2} I_0(r_2) & e^{-\alpha^2 t_2} J_0(r_2) & \cdots & e^{-\alpha^2 w^2 t_2} J_0(r_2) \\ \vdots & \vdots & \vdots & \ddots & \vdots \\ 1 & e^{\alpha^2 t_p} I_0(r_p) & e^{-\alpha^2 t_p} J_0(r_p) & \cdots & e^{-\alpha^2 w^2 t_p} J_0(r_p) \end{bmatrix}$, $\mathbf{B} = \begin{bmatrix} bb_1 & bb_2 & bb_3 & \cdots & bb_p \end{bmatrix}^{\mathrm{T}}$, and $\mathbf{C} = \begin{bmatrix} \overline{a}_0 & \overline{a}_k & \cdots & \overline{b}_w \end{bmatrix}^{\mathrm{T}}$. $\mathbf{A}$ is a matrix with dimensions $p \times q$, representing the basis functions. $\mathbf{C}$ is a vector with dimensions $q \times 1$, containing the unknown coefficients to be determined. $\mathbf{B}$ is a vector with dimensions $p \times 1$, representing the given boundary data at boundary collocation points. Here, p represents the number of boundary collocation points and q represents the number of terms associated with the order of the basis function, as described in Equation (23). These terms can be defined as follows: $r_1, r_2, \cdots, r_p$ represent the radii, $\overline{a}_0, \overline{a}_k, \cdots, \overline{b}_w$ are the unknown coefficients to be evaluated, and $bb_1, bb_2, bb_3, \cdots, bb_p$ represent the boundary data.

To solve Equation (23) and effectively determine the flow distribution within the spacetime domain, we must find the unknown coefficients that correspond to this three-dimensional spacetime domain. To achieve this, we introduce inner collocation points within the spacetime domain. By employing Equation (23), we can calculate the distribution at these inner collocation points within the spacetime domain.

2.3. Estimating Hydraulic Properties from Pumping Test

The pumping tests usually involve pumping from a single well and the groundwater heads are measured at the pumping well and observation wells over time. The curve-matching analysis, such as the log–log curve matching method, is usually adopted for estimating hydraulic properties [6,7,9]. However, the curve-matching procedure requires matching two graphical plots by hand or using commercially available computer programs [10,11].

Predicting the drawdown at a radial distance and time when the transmissivity, storativity, and pumping rate are known is called the forward problem. On the other hand, estimating hydraulic properties from the pumping test is categorized as an inverse problem in which the hydraulic properties are unknown. In this study, we revealed the estimation of hydraulic properties from a pumping test without using the conventional curve-matching method.

During a pumping test, the pumping rate is a known parameter. The well's geometry and the configuration of its boundaries are meticulously planned. However, certain hydraulic properties of an aquifer, such as transmissivity and storativity, remain unknown and need to be determined. Additionally, we collect measurements of groundwater levels at the observation well over various time intervals. These measured groundwater levels are also referred to as Dirichlet boundary data. Considering potential variations in instrument precision, a certain level of noise may exist. In this study, we accommodated this noise in the boundary data using the following equation:

$$\widetilde{B}_D = B_D \times \left[1 + \frac{\delta}{100} \times (2 \times rand - 1)\right], \tag{24}$$

where δ denotes the level of noise data, B_D denotes the actual Dirichlet boundary data, $\widetilde{B}_D$ denotes the Dirichlet boundary data with noise, and rand represents a random number generated using the *rand* command in MATLAB.

Since hydraulic properties are not given a priori, we adopted the iterative scheme named the fictitious time integration method (FTIM) to iteratively find the hydraulic properties. The solution procedure first involves a guess regarding the hydraulic properties, such as transmissivity and storativity. Because the hydraulic properties are not true values, the computed heads at the observation well are not consistence with the measured groundwater heads. The root-mean-square error (RMSE) of heads at the observation well is recorded. The advantage of utilizing RMSE in accuracy assessment lies in its ability to provide a quantitative, easily understood, and highly responsive measure of accuracy, which greatly simplifies the process of comparing models. These attributes have established RMSE as a widely used instrument for evaluating the precision of predictive models and measurements. The RMSE for the correction of the hydraulic properties using the FTIM is as follows:

$$T = T - \frac{\delta_t \nu_t}{\left(1+\tau_k^T\right)^m} \sqrt{\frac{\sum |h_C - h_O|^2}{n}},\ \tau_k^T = k\delta_t, \tag{25}$$

$$S = S - \frac{\delta_s \nu_s}{\left(1+\tau_k^S\right)^m} \sqrt{\frac{\sum |h_C - h_O|^2}{n}},\ \tau_k^S = k\delta_s, \tag{26}$$

where n is the number of data; δ_t and δ_s represent the time step sizes; v_t and v_s represent the non–zero coefficients; m represents a value in the range of zero to one; k represents the discrete time; and h_C and h_O represent the computed and observed heads, respectively. The iterative procedure of the FTIM ends when one of the following convergence criteria is achieved:

$$\sqrt{\frac{\sum |h_C - h_O|^2}{n}} \leq \varepsilon, \tag{27}$$

$$itn \geq \varepsilon_n, \tag{28}$$

where itn denotes the number of iterations, ε denotes convergence criteria, and ε_n denotes the maximum number of iterations. In this study, we considered $\varepsilon = 10^{-4}$ and $\varepsilon_n = 200$.

Figure 2 depicts the flowchart detailing the process for estimating hydraulic properties through pumping test analysis in this study. The flowchart outlines the step-by-step process for estimating the aquifer hydraulic properties from pumping test data.

2.4. Spacetime Collocation Scheme

The spacetime boundary-type meshless method is founded on the framework of the Minkowski spacetime domain. This domain is a fusion of a two-dimensional Euclidean space (Figure 3a) with a one-dimensional time dimension, resulting in a three-dimensional manifold (Figure 3b). As shown in Figure 3a, two types of collocation points containing the boundary collocation points and the source are placed in the two-dimensional space domain. Figure 3b shows the illustration of the three-dimensional spacetime domain. To efficiently utilize the collocation scheme within this Minkowski spacetime domain, the strategic placement of source points is of utmost importance. In the spacetime collocation scheme, these source points are located outside the boundaries of the spacetime domain, as shown in Figure 3.

Utilizing the proposed method, two sets of points are required: the boundary points and the source points. Boundary points are positioned along the well boundary, as indicated by yellow circular symbols, as well as in the infinite domain outside the well boundary, as represented by yellow triangular symbols. These boundary points serve the purpose of defining both the boundary conditions and initial conditions. Meanwhile, the source points, as denoted by small blue circular symbols, are positioned within the well boundary.

Within the spacetime collocation approach, we convert both the boundary and initial data into spacetime representations. This conversion allows for the original two-dimensional transient problem, which is initially formulated as an initial value problem, to be reformulated as a three-dimensional inverse boundary value problem. As a result, our method does not require the use of time-marching techniques.

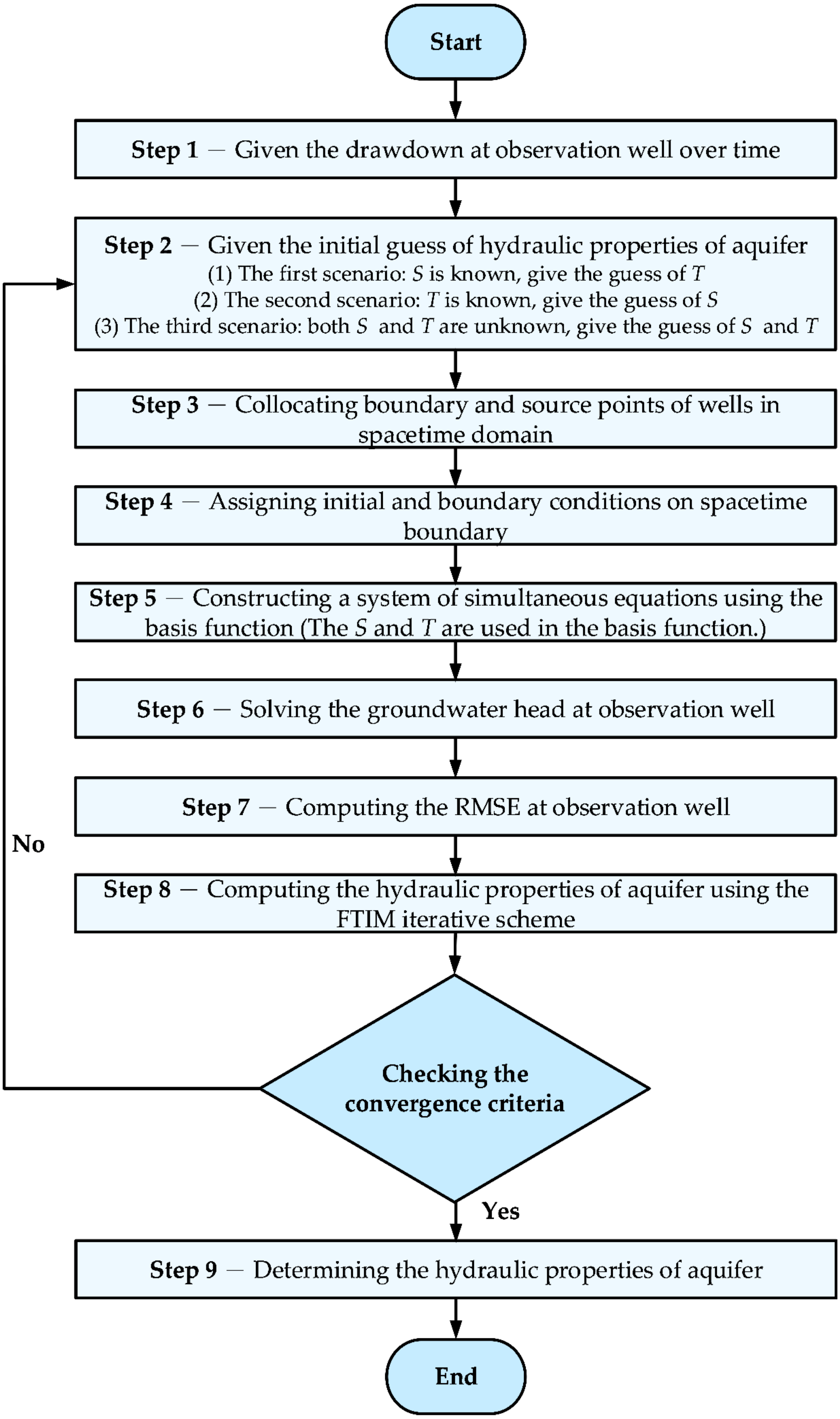

Figure 2. Flowchart for estimating hydraulic properties from pumping test analysis in this study.

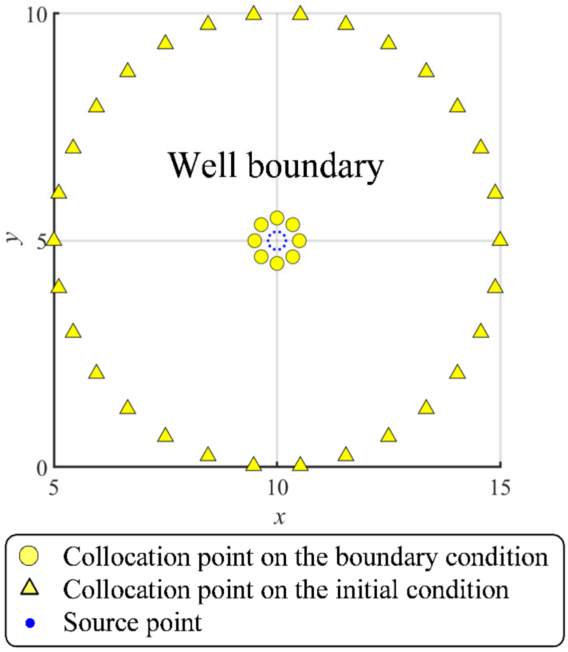

(**a**)

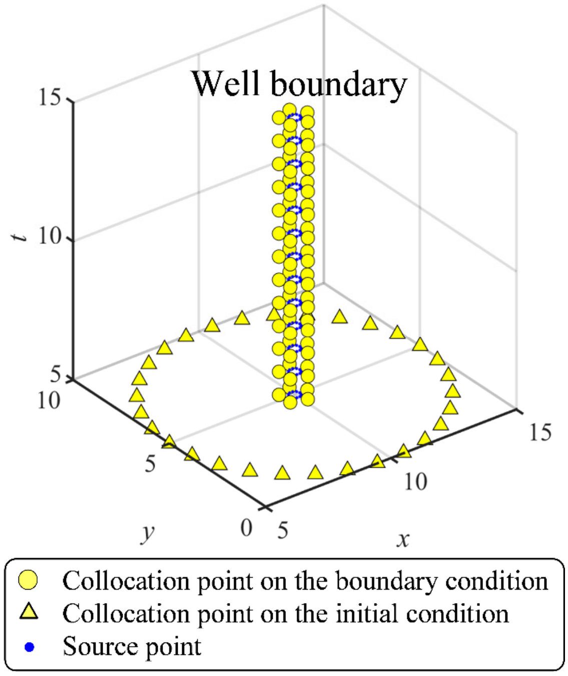

(**b**)

Figure 3. Illustration of the collocation points: (**a**) two-dimensional space domain; and (**b**) three-dimensional spacetime domain.

3. Validation Example

3.1. Modeling Radial Flow toward a Well in an Infinite Confined Aquifer

In the first validation example, we investigated a two-dimensional problem involving a transient flow problem to a well. This problem addressed by the Theis solution arises when a well is pumping water from an infinite confined aquifer. The objective was to determine how the pumping influences the groundwater levels and the rate at which water is drawn from the surrounding aquifer.

In the context of radial flow toward a well, Equation (1) represents the governing equation. The well's position was specified as (10, 5), with a well radius of 0.5 ft. A well located within a confined aquifer was scheduled to be pumped at a rate of 1500 ft^3/day for 10 days. The boundary configuration, as illustrated in Figure 3, was defined as follows:

$$\begin{array}{l} \partial\Omega = \{(x, y, t) | x = r(\theta)\cos\theta,\ y = r(\theta)\sin\theta,\ 5 \le t \le 15\}, \\ r(\theta) = 0.25\sin(8\theta),\ 0 \le \theta \le 2\pi, \end{array} , \tag{29}$$

where $\partial\Omega$ represents the boundary shape. The boundary data were established utilizing Equation (5), which corresponds to the Theis solution. The Theis solution assumes radial symmetry and homogeneous conditions, meaning that the aquifer properties are consistent throughout and the flow occurs in all directions away from the well equally. The Theis solution assumes the aquifer is infinite in extent, neglecting the influence of boundaries or obstacles. Using the Theis solution, one can estimate the drawdown at a given distance from the pumping well and assess the rate of groundwater extraction from the aquifer. In the pumping tests, Q = 1500 ft^3/day, $S = 3.5 \times 10^{-4}$, T = 525 ft^2/day, and w = 6.

Figure 3a presents the spatial arrangement of boundary and source points designed for simulating radial flow toward a well within a confined aquifer system. This setup includes a total of 255 source points and 1297 boundary points. The source points were situated within the pumping well. The boundary points were precisely aligned with the well boundaries and in the infinite domain (outside the well boundary), as shown in Figure 3b. Additionally, 1230 validation points were placed outside the well boundaries to assess the accuracy of the computed results. In the proposed spacetime collocation scheme, the boundary and initial data were transformed into spacetime data representations. This transformation enabled the reformulation of the original two-dimensional transient problem, which was initially formulated as an initial value problem. It was reformulated here as a three-dimensional inverse boundary value problem. Consequently, the proposed method does not rely on time-marching techniques, eliminating the need for iterative time-stepping calculations.

Figure 4 presents a comparison between the Theis solution and the computed drawdown at various times. The numerical solutions obtained through our proposed method align closely with the Theis solution. Additionally, comparisons of the results at specific time instances, namely, t = 5 days, t = 10 days, and t = 15 days, were evaluated.

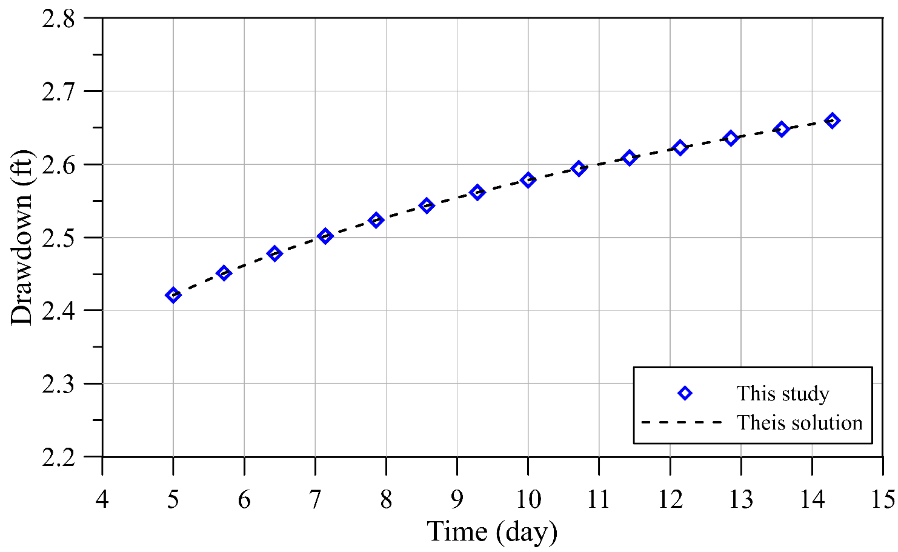

Figure 4. Comparison of Theis solution and computed drawdown versus time.

To assess the accuracy of the proposed method, the maximum absolute error was compared with the Theis solution. The obtained results reveal that the maximum absolute error fell within the order of 10^{-6}, signifying a high level of precision in the computed drawdown values.

3.2. Modeling Radial Flow toward Two Wells in an Infinite Confined Aquifer

In the second validation example, we explored a two-dimensional transient flow problem involving the influence of two wells. This scenario, addressed using the Theis solution, simulated a situation where two pumping wells were extracting water from an infinite confined aquifer. The primary objective was to assess how these pumping activities impact groundwater levels and the rate of water withdrawal from the surrounding aquifer. Focusing on the radial flow toward each well, we considered Equation (1) as the governing equation. The two pumping wells, denoted as well 1 and well 2, were positioned at coordinates (10, 5) and (15, 5), respectively. Each pumping well had a radius of 0.5 ft. Two wells located within a confined aquifer were scheduled to be pumped at a rate of 1500 ft^3/day and 500 ft^3/day for 10 days. Boundary conditions for this scenario were defined using the Theis solution, as represented by Equation (5), where $S = 3.5 \times 10^{-4}$, $T = 525$ ft^2/day, and $w = 6$.

The locations of these two pumping wells, each with its radius, were meticulously defined, as shown in Figure 5a. We utilized a spacetime collocation scheme that transformed the boundary and initial data into spacetime representations, as shown in Figure 5b. A total of 510 source points and 2471 boundary points were set. Figure 6 presents a comparison between the Theis solution and the computed drawdown at the final time. The numerical results obtained from our proposed method closely matched the Theis solution. The analysis of this case indicated that pumping well 1 had a higher pumping rate (1500 ft^3/day) compared with pumping well 2, which had a lower pumping rate (500 ft^3/day).

As a result, Figure 6 illustrates that the drawdown for pumping well 1 was larger, with a drawdown value of approximately −5.9 ft, while the drawdown for pumping well 2 was smaller, with a drawdown value of approximately −4.8 ft. Additionally, the drawdown near both pumping well 1 and pumping well 2 was influenced by the pumping rates of these wells, impacting their drawdown values. To evaluate the accuracy of the proposed method, we compared the maximum absolute error with the Theis solution. The results demonstrate that the maximum absolute error was within the range of 10^{-6}, demonstrating a remarkable level of precision in the computed drawdown values.

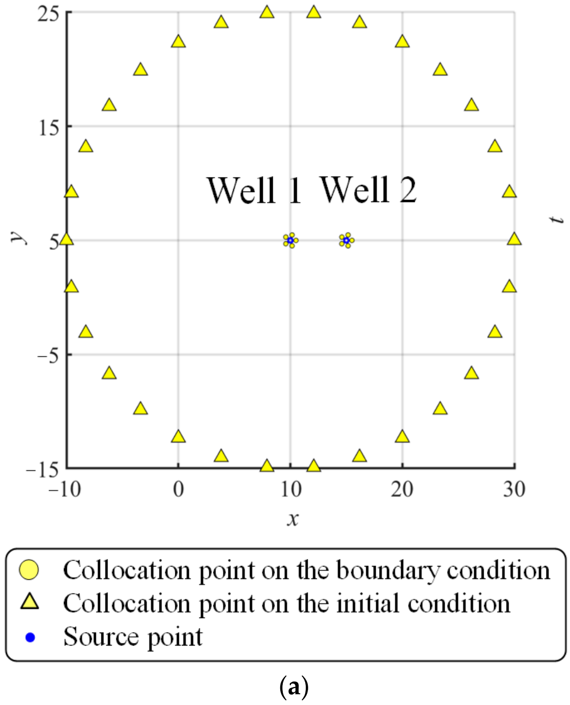

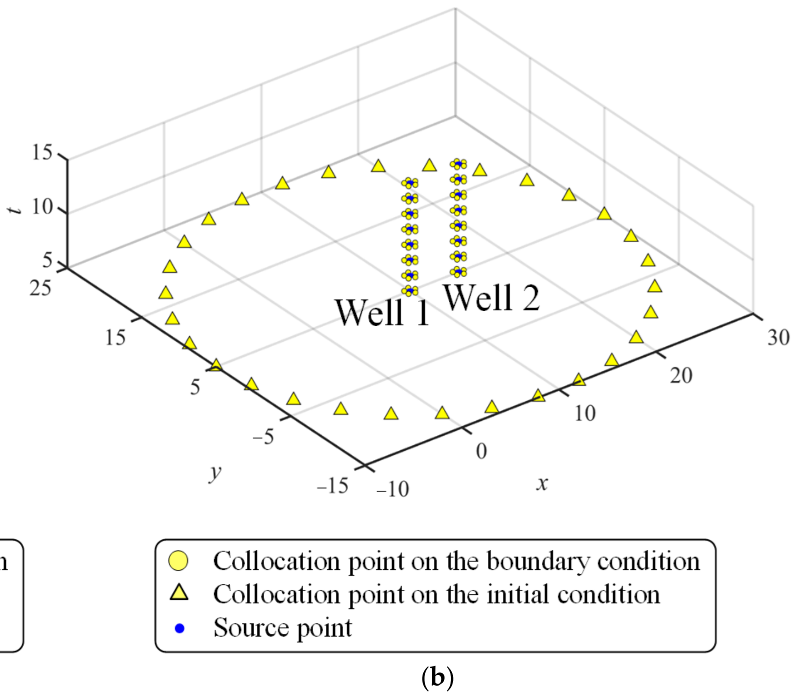

Figure 5. Location of the collocation points for the radial flow toward two pumping wells: (**a**) two-dimensional space domain; (**b**) three-dimensional spacetime domain.

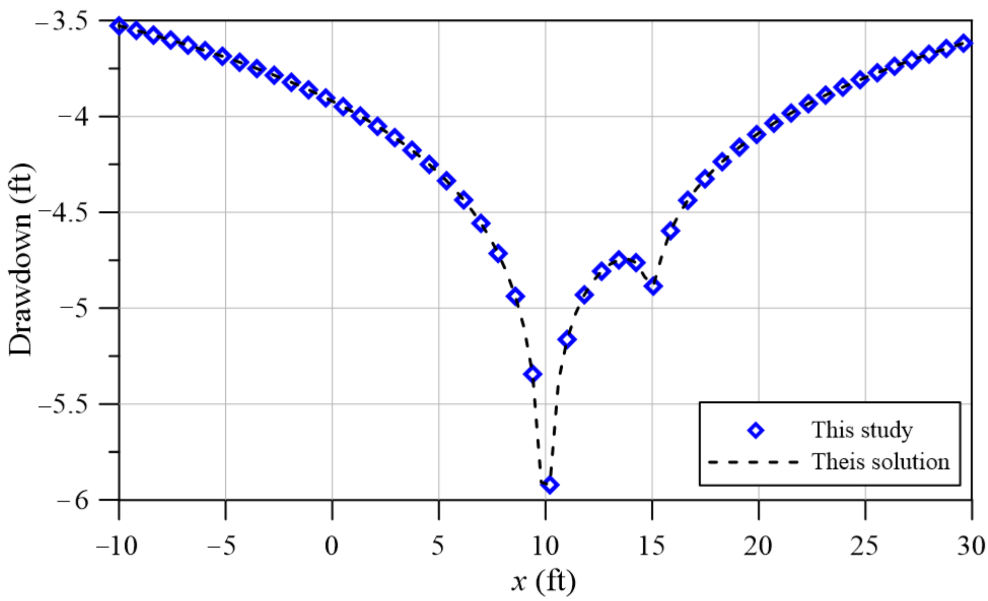

Figure 6. Comparison of the results for modeling radial flow toward two wells at $y = 0$.

3.3. Modeling Radial Flow toward Multiple Wells in an Infinite Confined Aquifer

In the third validation example, we explored a two-dimensional transient flow problem that examined the impact of four wells. Equation (1) is the governing equation. Two scenarios involving different placements of the four wells were considered, as depicted in Figure 7. Boundary conditions for this scenario were defined using the Theis solution, as represented by Equation (5), where $S = 3.5 \times 10^{-4}$, $T = 525\ \text{ft}^2/\text{day}$, and $w = 6$. The primary goal was to evaluate the effects of these pumping activities on groundwater levels and the rate of water extraction from the surrounding aquifer.

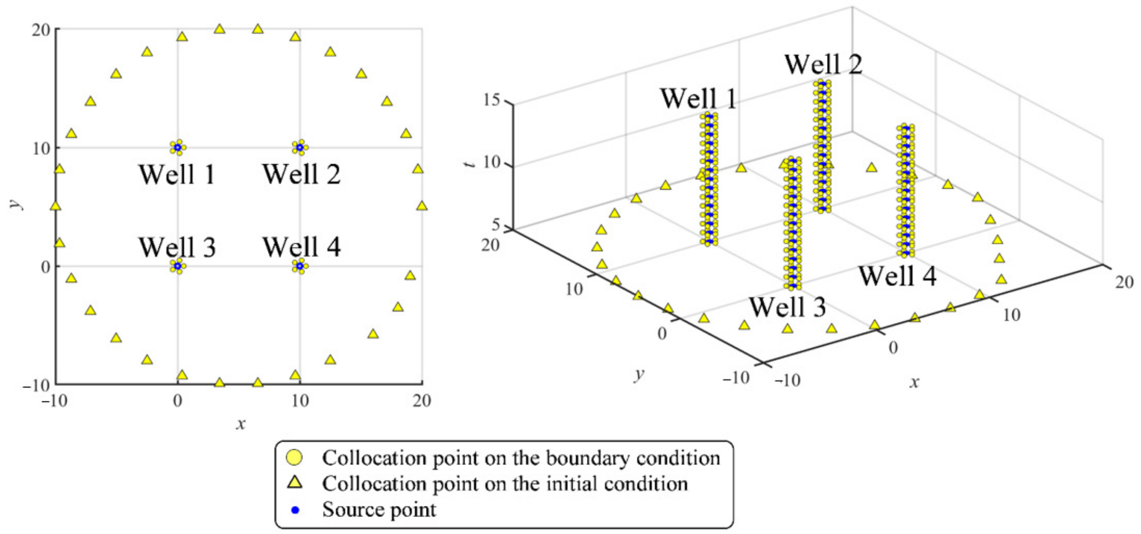

(**a**)

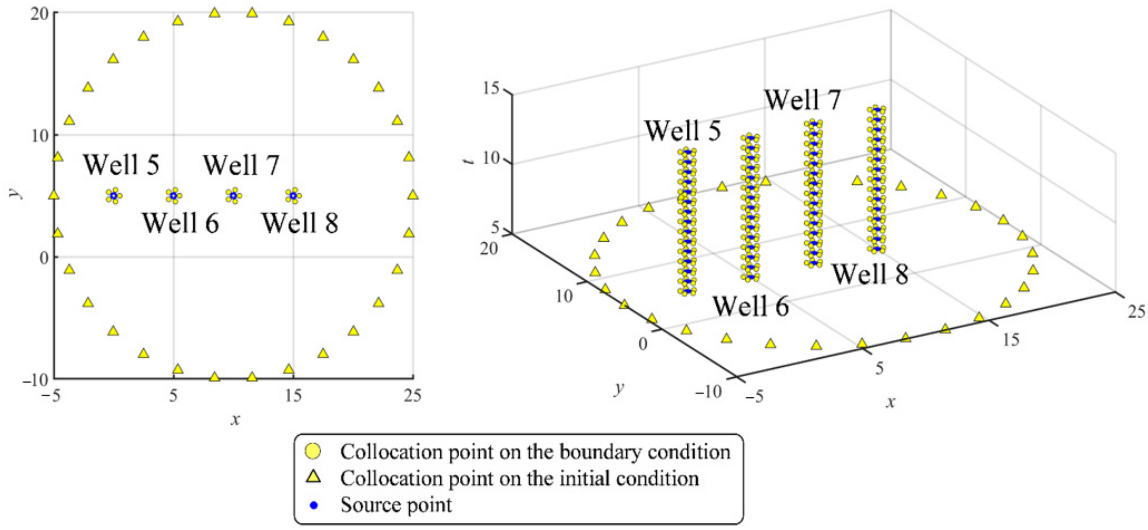

(**b**)

Figure 7. Collocation points for the radial flow toward four pumping wells: (**a**) case 1; (**b**) case 2.

(1) Case 1

In case 1, the four pumping wells, denoted as well 1, well 2, well 3, and well 4, were positioned at the coordinates (0, 10), (10, 10), (0, 0), and (10, 0), respectively. Each pumping well had a radius of 0.5 ft. Four wells situated within a confined aquifer were scheduled, as shown in Figure 7a, to be pumped at the same rate of $1500\ \text{ft}^3/\text{day}$ for 10 days.

(2) Case 2

In case 2, the four pumping wells, designated as well 5, well 6, well 7, and well 8, were situated at coordinates (0, 5), (5, 5), (10, 5), and (15, 5), respectively, each having a radius of

0.5 ft. These wells were located within a confined aquifer, as shown in Figure 7b, and were scheduled to undergo pumping at rates of 50, 1000, 1500, and 500 ft^3/day, each for 10 days.

A total of 1020 source points and 4942 boundary points were set. The source points were situated within the pumping wells, while the boundary points aligned with the well boundaries. Moreover, to evaluate the precision of our computed results, we introduced 1230 validation points thoughtfully placed outside the well boundaries.

Figure 8a shows a comparison between the drawdown results computed using our method and the Theis solution across varying distances from the four pumping wells in case 1. These results underscore the alignment between our approach and the Theis solution. The maximum absolute error was on the order of 10^{-6}, indicating a high level of precision in the computed drawdown values.

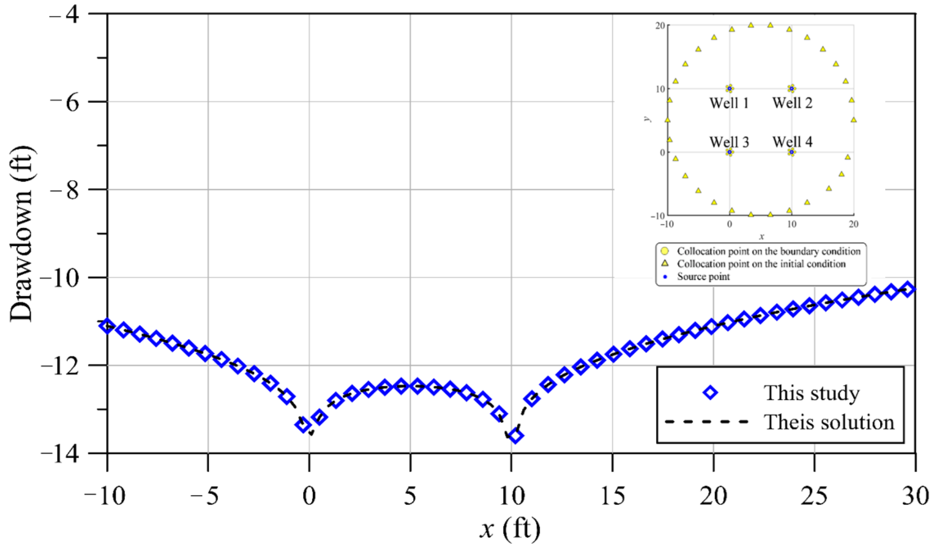

(**a**)

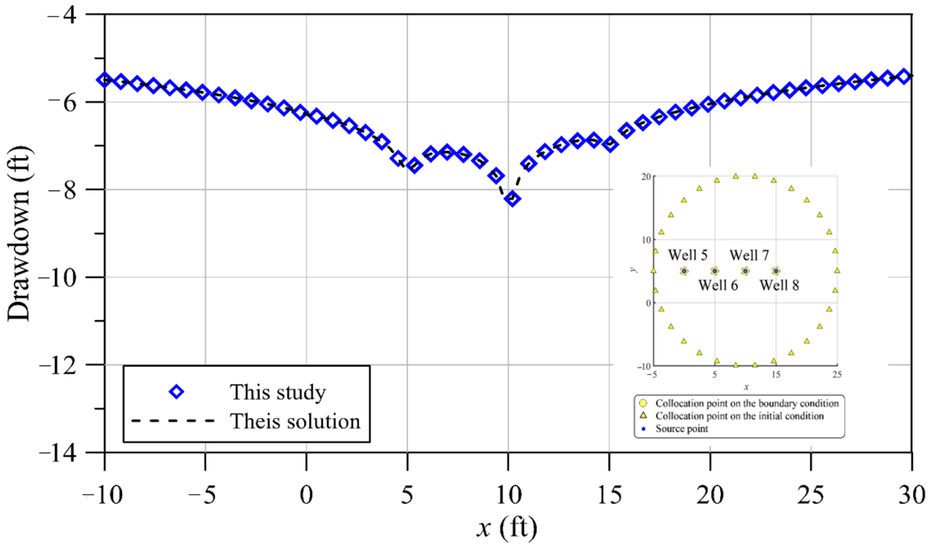

(**b**)

Figure 8. Comparison of the results for modeling radial flow toward four wells at $y = 0$: (**a**) case 1; (**b**) case 2.

Figure 8b presents a comparison of the drawdown results between our method and the Theis solution at different distances from the four pumping wells in case 2. These results highlight the consistency between our approach and the Theis solution. The maximum absolute error was in the order of 10^{-6}, signifying a remarkably high level of precision in the computed drawdown values.

4. Application

4.1. Estimating Aquifer Hydraulic Properties from a Pumping Test with One Well

As shown in the following analysis, three scenarios of estimating aquifer hydraulic properties through pumping tests were carried out. The first scenario involved a known storativity, requiring the estimation of the transmissivity. The second scenario involved a known transmissivity, requiring the estimation of the storativity. The third scenario entailed both the storativity and transmissivity being unknown, requiring the estimation of both parameters, i.e., storativity and transmissivity.

(1) The First Scenario: Estimation of Transmissivity

The first scenario under investigation involved estimating the transmissivity of an aquifer through pumping tests. The pumping rate Q and storativity S were 1500 ft^3/day and 3×10^{-4}, respectively. The target value of the transmissivity T was 525 ft^2/day. The identification process started with an initial assumption for the unknown transmissivity T since the number of unknown parameters was one. It concluded once the specified stopping criteria, as shown in Equations (27) and (28), were met. The initial assumption of the transmissivity T was 1700 ft^2/day.

The boundary configuration is illustrated in Figure 3. The boundary data were established utilizing Equation (5). A set of data points, consisting of 255 source points and 1297 boundary points, was positioned. The source points were specifically located within the confines of the pumping well, while the boundary points were aligned with the precise boundaries of the well. Furthermore, to evaluate the precision of our computed results, we assigned an additional 1230 validation points strategically positioned outside the well boundaries. The numerical parameters $w = 6$, $\delta_t = 1$, $v_t = 1$, and $m = 0.01$ were considered in this numerical implementation. The aquifer parameters could be estimated by minimizing the sum of the squared errors between the observed and predicted drawdowns. This optimization process was achieved using Equation (25).

Figure 9 displays the temporal evolution of the estimated transmissivity. The results illustrate an initial fluctuation in the first few iterations, which stabilized to a constant value after 11 iterations. The parameter estimation indicated that the estimated transmissivity was accurately identified after 11 iterations.

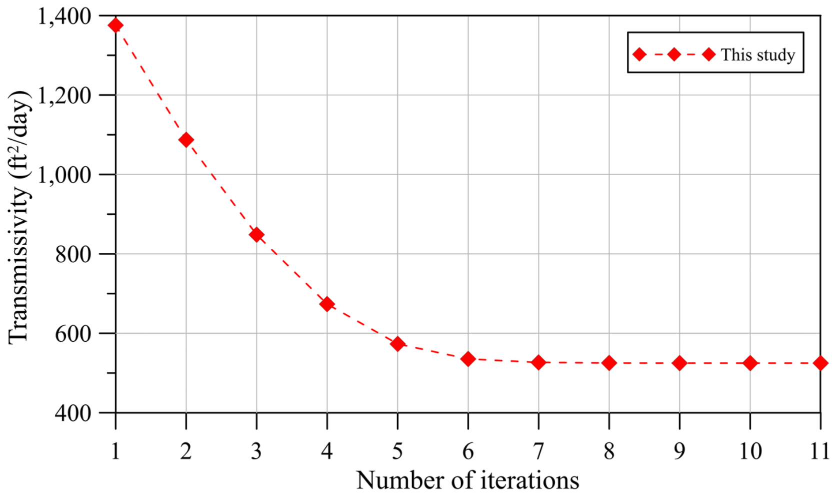

Figure 9. Estimated transmissivity versus number of iterations for a pumping test with one well (the first scenario).

To evaluate the stability of the proposed method, we considered the input measured data contaminated by random noise. The levels of noise were selected to be $\delta = 0$ and δ

= 0.1. Figure 10 illustrates a comparison between the Theis solution and the computed drawdown for δ = 0 and δ = 0.1 at different time intervals. The maximum absolute errors for δ = 0 and δ = 0.1 were 10^{-3} and 10^{-2}, respectively. The analysis revealed a close alignment between the computed drawdown and the Theis solution. Moreover, the results indicate that even when considering the potential influence of noise on the boundary conditions, our method consistently delivered high-precision outcomes, demonstrating its robustness against noise interference.

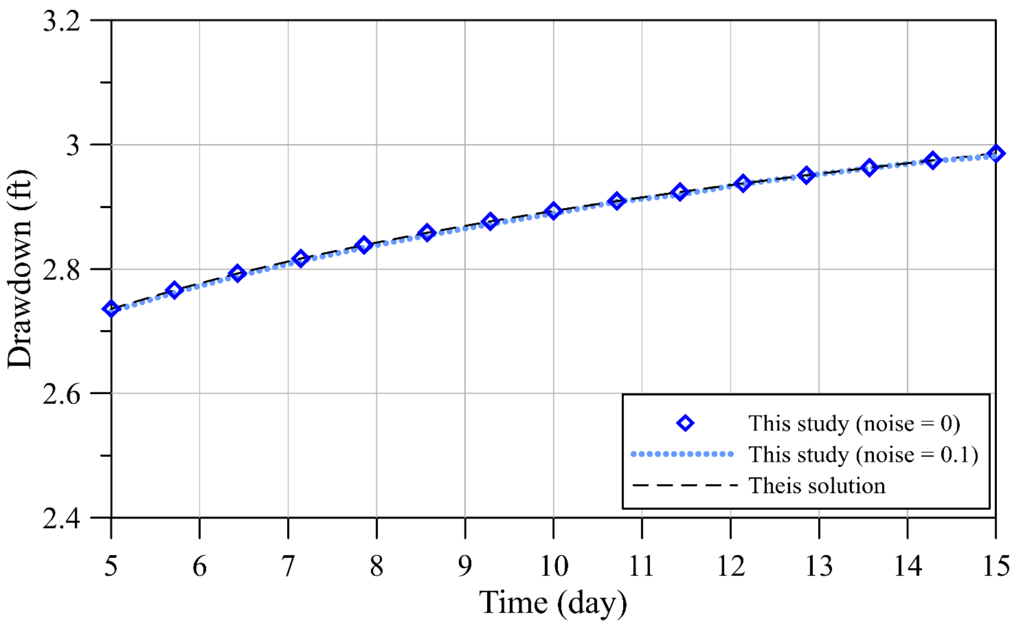

Figure 10. Comparison of computed drawdown and Theis solution for a pumping test with one well (the first scenario).

(2) The Second Scenario: Estimation of Storativity

The second scenario involved estimating the storativity of an aquifer using pumping tests. The pumping rate Q and transmissivity T were 3000 ft^3/day and 525 ft^2/day, respectively. The target value of the storativity S was 3.5×10^{-4}. The identification process started with an initial assumption for the unknown storativity S since the number of unknown parameters was one. It concluded once the specified stopping criteria were met. The initial assumption of the storativity S was 5×10^{-4}.

The boundary configuration is illustrated in Figure 3. The boundary data were established utilizing Equation (5). A set of data points, consisting of 225 source points and 1297 boundary points, was positioned. The source points were specifically located within the confines of the pumping well, while the boundary points were aligned with the precise boundaries of the well. Furthermore, to evaluate the precision of our computed results, we assigned an additional 1215 validation points strategically positioned outside the well boundaries. The numerical parameters w = 6, $\delta_t = 1$, $v_t = 1$, and $m = 0.01$ were considered in this numerical implementation. The aquifer parameters can be estimated by minimizing the sum of the squared errors between the observed and predicted drawdowns. This optimization process was achieved using Equation (26).

Figure 11 displays the temporal evolution of the estimated storativity. The results illustrate an initial fluctuation in the first few iterations, which stabilized to a constant value after 17 iterations. The parameter estimation indicates that the estimated storativity was accurately identified after 17 iterations.

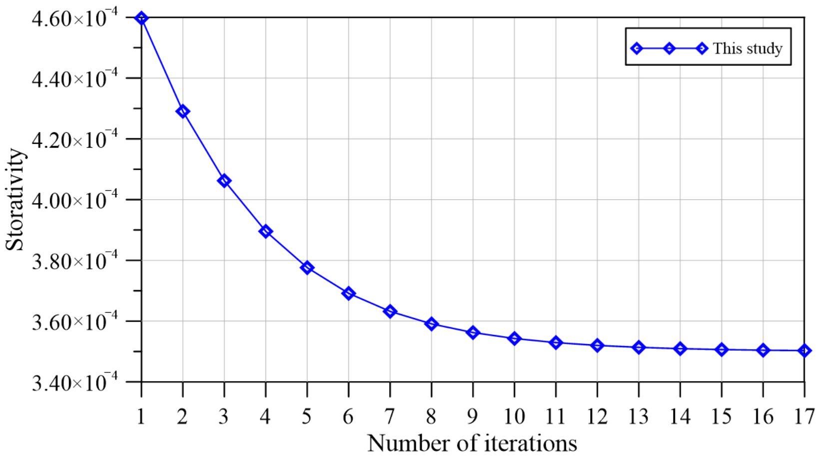

Figure 11. Estimated storativity versus number of iterations for a pumping test with one well (the second scenario).

To evaluate the stability of the proposed method, we considered that the input measured data were contaminated by random noise. The levels of noise were selected to be $\delta = 0$ and $\delta = 0.1$. Figure 12 illustrates a comparison between the Theis solution and the computed drawdown for $\delta = 0$ and $\delta = 0.1$ at different time intervals. The maximum absolute errors for $\delta = 0$ and $\delta = 0.1$ were 10^{-3} and 10^{-2}, respectively. It appears that the computed drawdown closely matched the Theis solution.

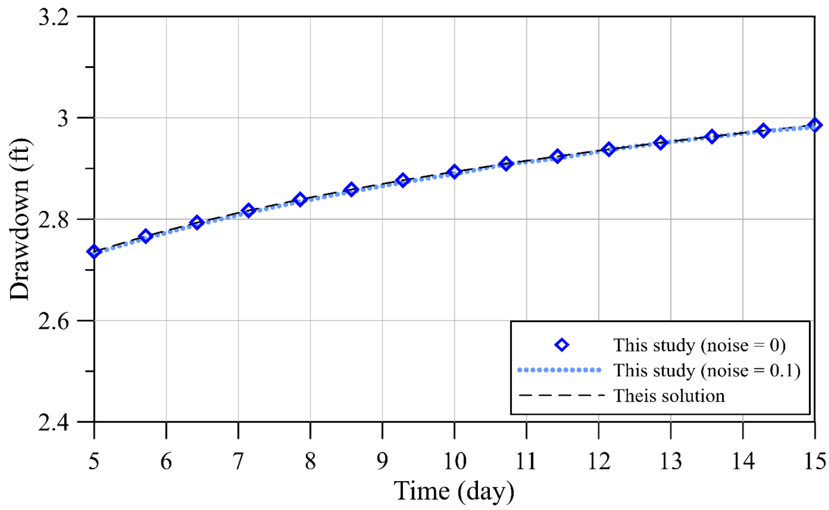

Figure 12. Comparison of computed drawdown and Theis solution for a pumping test with one well (the second scenario).

(3) The Third Scenario: Estimation of Transmissivity and Storativity

The third scenario involved estimating the storativity and transmissivity of an aquifer using pumping tests. We considered both the storativity and transmissivity as being unknown, requiring the estimation of both parameters, i.e., storativity and transmissivity.

The pumping rate Q was 1500 ft^3/day. The target values of the transmissivity T and storativity S were 525 ft^2/day and 3×10^{-4}, respectively. The identification process started with an initial assumption for the unknown transmissivity T and storativity S since the number of unknown parameters was two. It concluded once the specified stopping criteria were met. The initial assumption of the transmissivity T and storativity S were 1700 ft^2/day and 5×10^{-4}, respectively.

The boundary configuration is illustrated in Figure 3. The boundary data were established utilizing Equation (5). A set of data points, consisting of 225 source points and

1297 boundary points, was positioned. The source points were specifically located within the confines of the pumping well, while the boundary points were aligned with the precise boundaries of the well. Furthermore, to evaluate the precision of our computed results, we assigned an additional 1215 validation points that were strategically positioned outside the well boundaries. The numerical parameters $w = 6$, $\delta_t = 1$, $v_t = 1$, and $m = 0.01$ were considered in this numerical implementation. The aquifer parameters could be estimated by minimizing the sum of the squared errors between the observed and predicted drawdowns. This optimization process was achieved using Equations (25) and (26).

Figure 13 displays the temporal evolution of the estimated transmissivity and storativity. The results illustrate an initial fluctuation in the first few iterations, which stabilized to a constant value after 10 iterations. The parameter estimation indicates that the estimated transmissivity was accurately identified after 10 iterations.

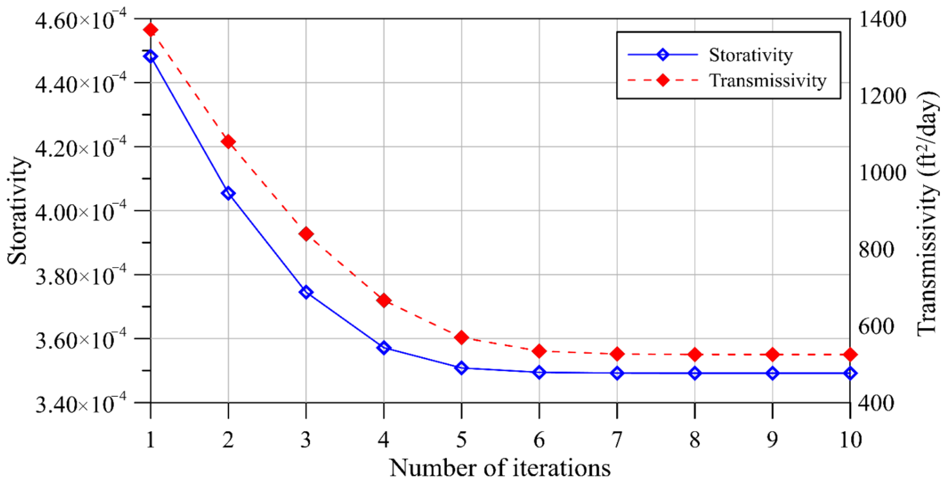

Figure 13. Estimated storativity and transmissivity versus number of iterations for a pumping test with one well (the third scenario).

To evaluate the stability of the proposed method, we considered that the input measured data were contaminated by random noise. The levels of noise were selected to be $\delta = 0$ and $\delta = 0.01$. Figure 14 illustrates a comparison between the Theis solution and the computed drawdown for $\delta = 0$ and $\delta = 0.01$ at different time intervals. The maximum absolute errors for $\delta = 0$ and $\delta = 0.1$ were 10^{-5} and 10^{-4}, respectively. It appears that the computed drawdown closely matched the Theis solution.

4.2. Estimating Aquifer Hydraulic Properties from a Pumping Test with Two Wells

This example under investigation involved estimating the transmissivity of an aquifer from a pumping test with two wells. Focusing on the radial flow toward each well, we considered Equation (1) as the governing equation. The two pumping wells, denoted as well 1 and well 2, were positioned at coordinates (10, 5) and (15, 5), respectively. Each pumping well had a radius of 0.5 ft. Two wells located within a confined aquifer were scheduled to be pumped at a rate of 1500 ft^3/day and 500 ft^3/day for 10 days. The boundary configuration is illustrated in Figure 5.

The scenario involved a known storativity, requiring the estimation of transmissivity. The storativity S was 3×10^{-4}. The target value of the transmissivity T was 525 ft^2/day. The identification process started with an initial assumption for the unknown transmissivity T since the number of unknown parameters was one. It concluded once the specified stopping criteria were met. The initial assumption of the transmissivity T was 90 ft^2/day.

We positioned a set of data points, consisting of 510 source points and 2471 boundary points, with careful attention to their placement accuracy. The source points were specifically located within the confines of the pumping well, while the boundary points were aligned with the precise boundaries of the well. Furthermore, to evaluate the precision of our computed results, we assigned an additional 1215 validation points strategically positioned outside the well boundaries. The numerical parameters $w = 6$, $\delta_t = 1$, $v_t = 1$, and $m = 0.01$ were considered in this numerical implementation. The aquifer parameters could be estimated by minimizing the sum of the squared errors between the observed and predicted drawdowns. This optimization process was achieved using Equation (25).

Figure 15 displays the temporal evolution of the estimated transmissivity. The results illustrate an initial fluctuation in the first few iterations, which stabilized to a constant value after 16 iterations. The parameter estimation indicated that estimated transmissivity was accurately identified after 16 iterations. Figure 16 presents a comparison between the Theis solution and the computed drawdown, with a maximum absolute error of 10^{-6}. The results demonstrate a close alignment between the computed drawdown and the Theis solution.

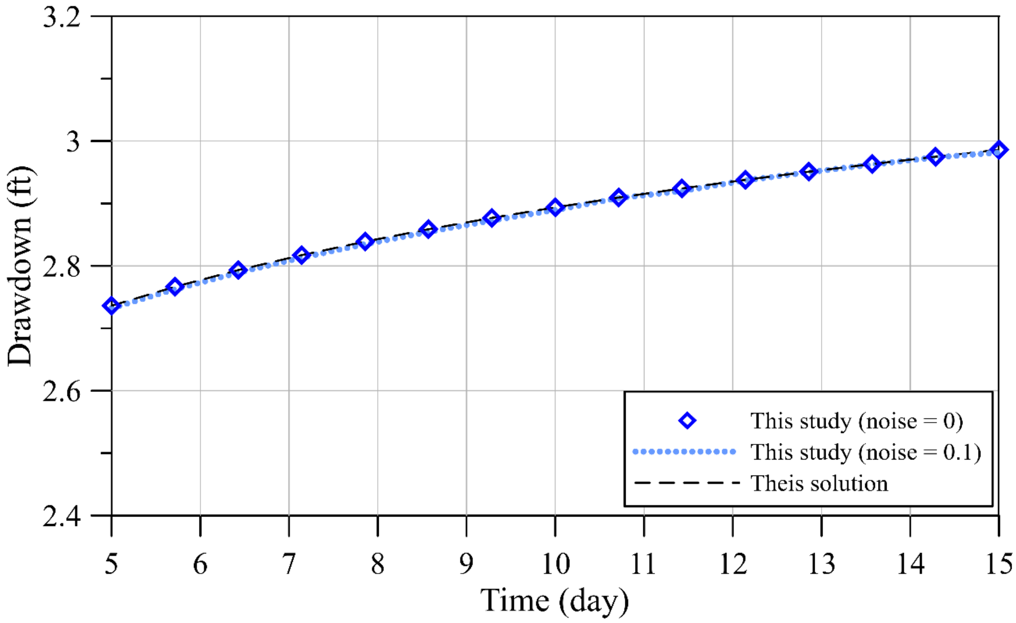

Figure 14. Comparison of computed drawdown and Theis solution for a pumping test with one well (the third scenario).

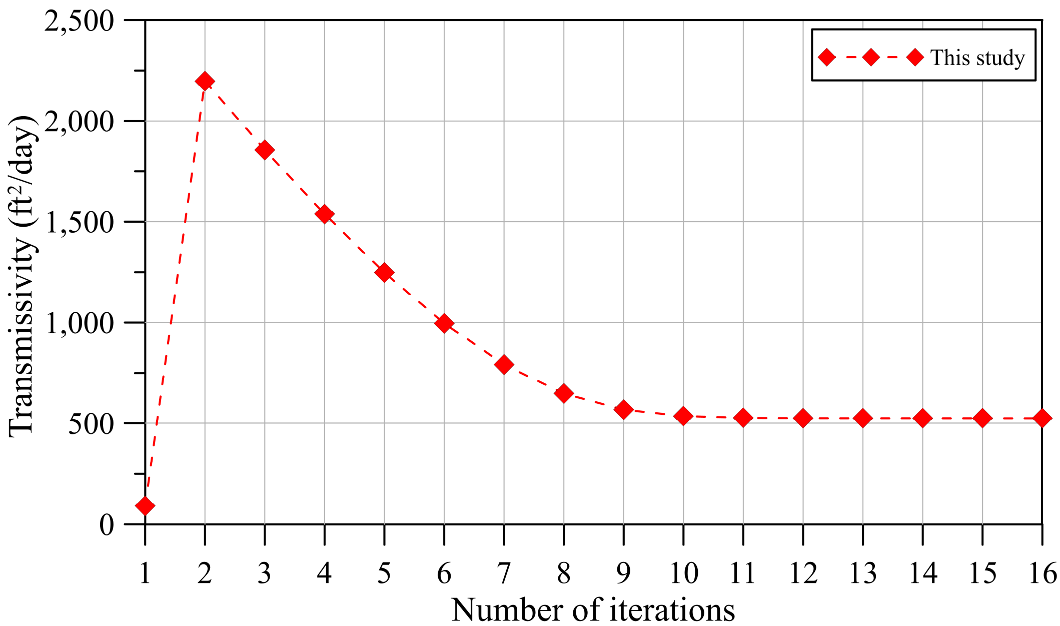

Figure 15. Estimated transmissivity versus number of iterations for a pumping test with two wells.

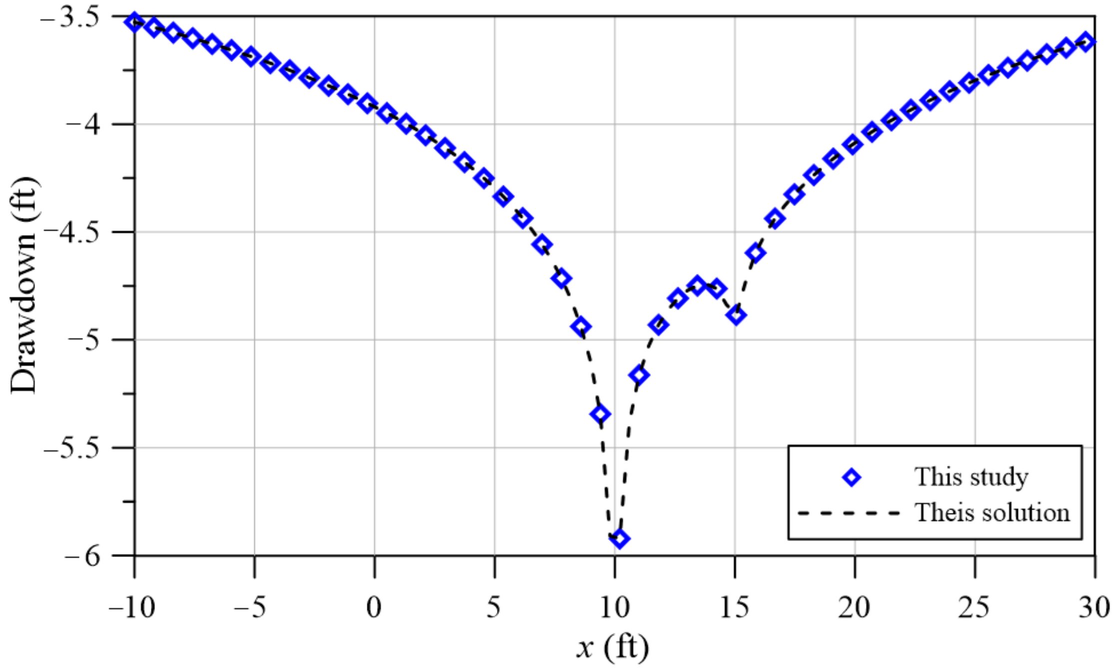

Figure 16. Comparison of computed drawdown and Theis solution for a pumping test with two wells.

4.3. Estimating Aquifer Hydraulic Properties from a Pumping Test with Four Wells

The final example involved estimating the transmissivity of an aquifer from a pumping test with two wells. Focusing on the radial flow toward each well, we considered Equation (1) as the governing equation. The four pumping wells, designated as well 5, well 6, well 7, and well 8, were situated at coordinates (0, 5), (5, 5), (10, 5), and (15, 5), respectively, with each having a radius of 0.5 ft. These wells were located within a confined aquifer, as shown in Figure 7b, and were scheduled to undergo pumping at rates of 50, 1000, 1500, and 500 ft^3/day, each for 10 days.

The scenario involves known storativity, requiring the estimation of transmissivity. The storativity S was 3×10^{-4}. The target value of the transmissivity T was 525 ft^2/day. The identification process started with an initial assumption for the unknown transmissivity T since the number of unknown parameters was one. It concluded once the specified stopping criteria were met. The initial assumption of the transmissivity T was 25 ft^2/day.

A total of 1020 source points and 4942 boundary points were set. The source points were situated within the pumping wells, while the boundary points aligned with the well boundaries. Moreover, to evaluate the precision of our computed results, we introduced 1230 validation points that were thoughtfully placed outside the well boundaries. The numerical parameters $w = 6$, $\delta_t = 1$, $v_t = 1$, and $m = 0.01$ were considered in this numerical implementation. The aquifer parameters could be estimated by minimizing the sum of the squared errors between the observed and predicted drawdowns. This optimization process was achieved through Equation (25).

Figure 17 displays the temporal evolution of the estimated transmissivity. The results illustrate an initial fluctuation in the first few iterations, which stabilized to a constant value after 26 iterations. The parameter estimation indicates that the estimated transmissivity was accurately identified after 26 iterations. Figure 18 presents a comparison between the Theis solution and the computed drawdown, with a maximum absolute error of 10^{-6}. The results demonstrate a close alignment between the computed drawdown and the Theis solution.

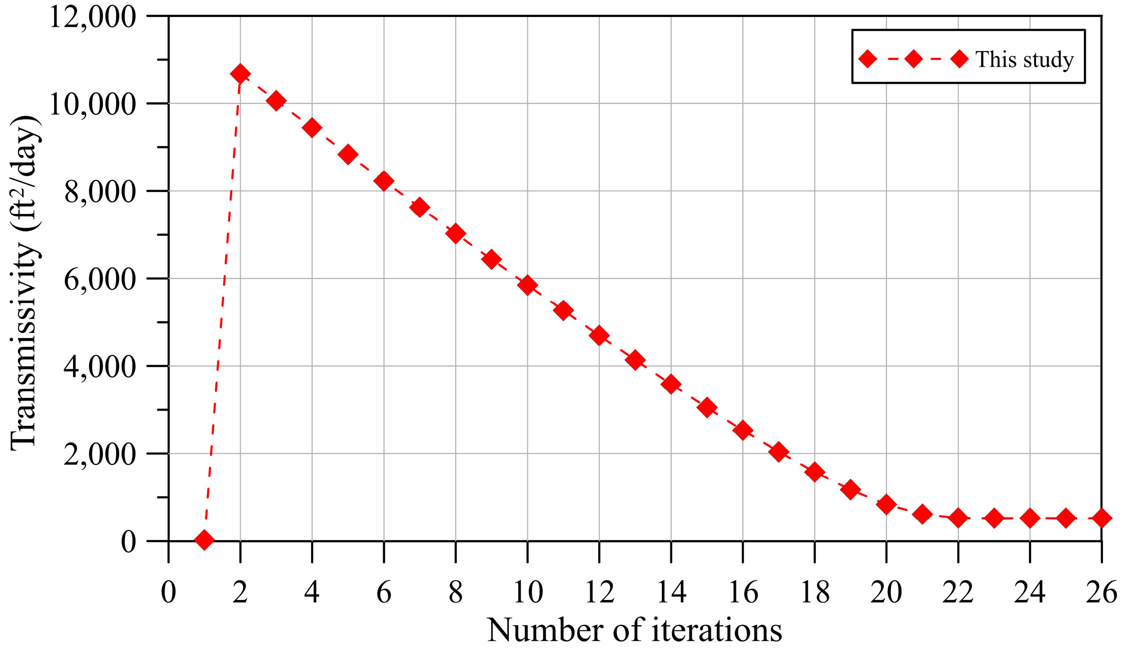

Figure 17. Estimated transmissivity versus number of iterations for a pumping test with four wells.

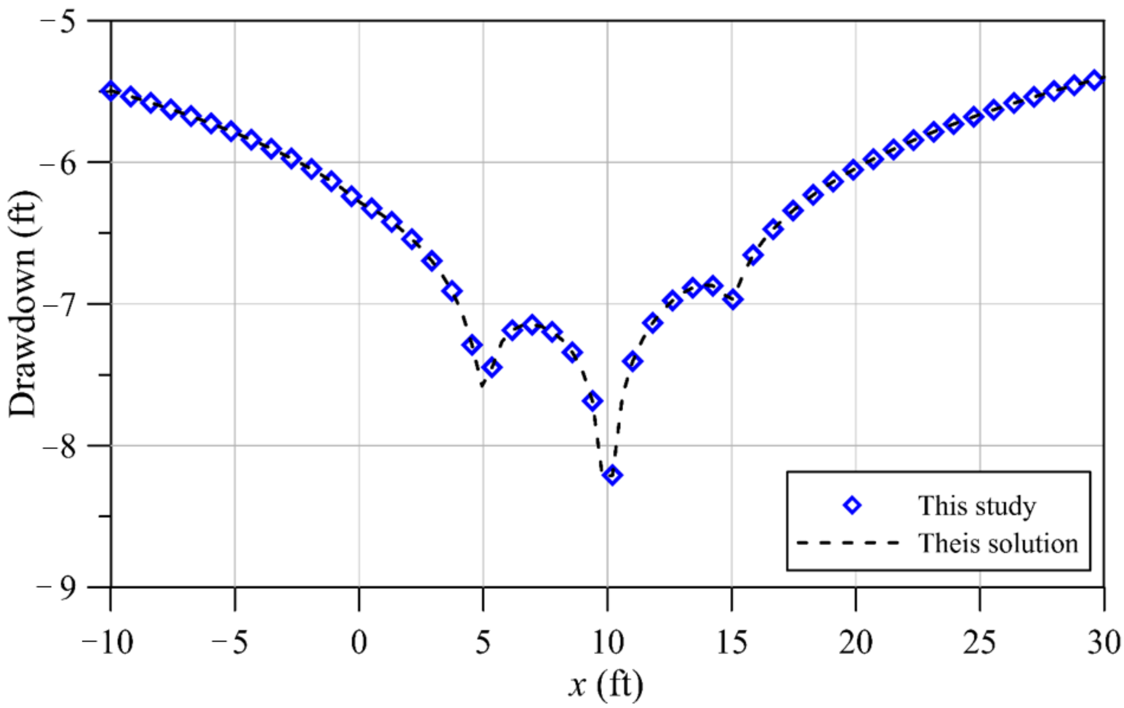

Figure 18. Comparison of computed drawdown and Theis solution for a pumping test with four wells.

5. Discussion

This study emphasized the importance of adopting a spacetime domain approach, which allows for the application of initial and boundary data to spacetime boundary collocation points. We conducted three validations by comparing our results with the Theis solution, and the outcomes demonstrate a high level of accuracy. Furthermore, we applied this method to estimate aquifer hydraulic properties using pumping tests, employing an iterative fictitious time integration method in three different scenarios. The simultaneous temporal and spatial discretization within the spacetime domain offers distinct advantages in determining hydraulic properties, including transmissivity and storativity. Even when dealing with input data affected by random noise, our method closely aligns with the Theis solution, showing its effectiveness in identifying transmissivity and storativity, particularly when it stabilizes.

While conventional finite element or finite difference methods can be used to address axisymmetric flow problems, they demand the use of highly dense meshes and longer computational durations to achieve the desired level of accuracy. In contrast, our method offers significant benefits, as it does not rely on mesh generation. Instead, it emphasizes boundary discretization, leading to a notable reduction in computational complexity.

Nevertheless, the proposed method may only be limited to assessing axisymmetric transient groundwater flow problems under the assumptions of homogeneity aquifer. Further investigations are recommended to explore the method's performance when applied to model groundwater flow in heterogeneous porous media. These investigations would provide a more comprehensive understanding of the method's suitability for addressing real-world groundwater issues.

6. Conclusions

This article presents an innovative spacetime boundary-type meshless method designed to address axisymmetric transient groundwater flow problems. The study highlights the significance of employing a spacetime domain framework, enabling the application of initial and boundary data on spacetime boundary collocation points. The key findings and conclusions are summarized as follows:

(1) The proposed method demonstrated its robustness and accuracy in approximating solutions using basis functions, addressing inverse boundary value problems. Utilizing a spacetime collocation scheme, our method emphasizes boundary discretization, leading to a notable reduction in computational complexity.

(2) Three validations were achieved using comparisons with the Theis solution. Our findings reveal a maximum absolute error on the order of 10^{-7}, underscoring the remarkable precision achieved in our computed drawdown values. Our method particularly excelled in predicting drawdown near pumping wells, consistently delivering highly accurate results without reliance on conventional time-marching schemes. It highlights that the proposed method aligns with the characteristics of a boundary discretization numerical approach and effectively minimizes computational complexity.

(3) Moreover, we further applied the proposed method for estimating aquifer hydraulic properties using pumping tests, conducting three scenarios with an iterative fictitious time integration method. The simultaneous temporal and spatial discretization within the spacetime domain was found to be advantageous for determining hydraulic properties, including transmissivity and storativity. Even when considering input data contaminated by random noise, our method closely matched the Theis solution, showing its capability to identify transmissivity and storativity effectively, particularly when it stabilized.

(4) However, it is worth noting that the proposed method may have limitations, as it is currently best suited for evaluating axisymmetric transient groundwater flow problems under the assumption of a homogeneous aquifer. Further enhancements are recommended to investigate how the method performs when modeling groundwater flow in heterogeneous porous media.

Author Contributions: Conceptualization, editing, and supervision, C.-Y.K.; methodology, investigation, and writing the original draft, C.-Y.L. All authors have read and agreed to the published version of the manuscript.

Funding: This research received no external funding.

Data Availability Statement: Research data are available on request.

Conflicts of Interest: The authors declare no conflict of interest.

References

1. Amanambu, A.C.; Obarein, O.A.; Mossa, J.; Li, L.; Ayeni, S.S.; Balogun, O.; Oyebamiji, A.; Ochege, F.U. Groundwater system and climate change: Present status and future considerations. *J. Hydrol.* **2020**, *589*, 125163. [CrossRef]
2. McDonough, L.K.; Santos, I.R.; Andersen, M.S.; O'Carroll, D.M.; Rutlidge, H.; Meredith, K.; Oudone, P.; Bridgeman, J.; Gooddy, D.C.; Sorensen, J.P.R.; et al. Changes in global groundwater organic carbon driven by climate change and urbanization. *Nat. Commun.* **2020**, *11*, 1279. [CrossRef] [PubMed]
3. Chang, J.; Wang, G.; Mao, T. Simulation and prediction of suprapermafrost groundwater level variation in response to climate change using a neural network model. *J. Hydrol.* **2015**, *529*, 1211–1220. [CrossRef]
4. Avci, C.B.; Ufuk Sahin, A. Assessing radial transmissivity variation in heterogeneous aquifers using analytical techniques. *Hydrol. Process.* **2014**, *28*, 5739–5754. [CrossRef]
5. Selvadurai, A.P.S.; Jenner, L. Radial flow permeability testing of an argillaceous limestone. *Groundwater* **2013**, *51*, 100–107. [CrossRef]
6. Haitjema, H. The role of hand calculations in ground water flow modeling. *Groundwater* **2006**, *44*, 786–791. [CrossRef]
7. Birhanu, Z.K.; Kitterød, N.O.; Krogstad, H.; Kværnø, A. Analytical and numerical solutions of radially symmetric aquifer thermal energy storage problems. *Hydrol. Earth Syst. Sci. Discuss.* **2017**, 1–19.
8. Waghmare, R.V. Mathematical modeling of flow in confined aquifer. *Int. J. Nov. Res. Phys. Chem. Math.* **2016**, *3*, 1–16.
9. Lin, Y.C.; Li, M.H.; Yeh, H.D. An analytical model for flow induced by a constant-head pumping in a leaky unconfined aquifer system with considering unsaturated flow. *Adv. Water Resour.* **2017**, *107*, 525–534. [CrossRef]
10. Kumbhakar, M.; Singh, V.P. Analytical Approximations of Well Function by Solving the Governing Differential Equation Representing Unsteady Groundwater Flow in a Confined Aquifer. *Mathematics* **2023**, *11*, 1652. [CrossRef]
11. Flores, L.; Bailey, R.T. Revisiting the Theis solution derivation to enhance understanding and application. *Hydrogeol. J.* **2019**, *27*, 55–60. [CrossRef]
12. Seyedpour, S.M.; Valizadeh, I.; Kirmizakis, P.; Doherty, R.; Ricken, T. Optimization of the groundwater remediation process using a coupled genetic algorithm-finite difference method. *Water* **2021**, *13*, 383. [CrossRef]
13. Omar, P.J.; Gaur, S.; Dwivedi, S.B.; Dikshit, P.K.S. Groundwater modelling using an analytic element method and finite difference method: An insight into lower ganga river basin. *J. Earth Syst. Sci.* **2019**, *128*, 195. [CrossRef]
14. Tamayo-Mas, E.; Bianchi, M.; Mansour, M. Impact of model complexity and multi-scale data integration on the estimation of hydrogeological parameters in a dual-porosity aquifer. *Hydrogeol. J.* **2018**, *26*, 1917–1933. [CrossRef]
15. Zhang, L.; Zhao, L.; Yang, L.; Songtao, H. Analyses on soil temperature responses to intermittent heat rejection from BHEs in soils with groundwater advection. *Energy Build.* **2015**, *107*, 355–365. [CrossRef]
16. Wu, L.Z.; Zhu, S.R.; Peng, J. Application of the Chebyshev spectral method to the simulation of groundwater flow and rainfall-induced landslides. *Appl. Math. Model.* **2020**, *80*, 408–425. [CrossRef]
17. Patel, S.; Rastogi, A.K. Meshfree multiquadric solution for real field large heterogeneous aquifer system. *Water Resour. Manag.* **2017**, *31*, 2869–2884. [CrossRef]
18. Guneshwor, L.; Eldho, T.I.; Vinod Kumar, A. Identification of groundwater contamination sources using meshfree RPCM simulation and particle swarm optimization. *Water Resour. Manag.* **2018**, *32*, 1517–1538. [CrossRef]
19. Wang, Q.; Kim, P.; Qu, W. A hybrid localized meshless method for the solution of transient groundwater flow in two dimensions. *Mathematics* **2022**, *10*, 515. [CrossRef]
20. Li, J.; Chen, Y.; Pepper, D. Radial basis function method for 1-D and 2-D groundwater contaminant transport modeling. *Comput. Mech.* **2003**, *32*, 10–15. [CrossRef]
21. Lin, G.F.; Chen, L.H. Time series forecasting by combining the radial basis function network and the self-organizing map. *Hydrol. Process. Int. J.* **2005**, *19*, 1925–1937. [CrossRef]
22. Kovářík, K.; Mužík, J. A meshless solution for two dimensional density-driven groundwater flow. *Eng. Anal. Bound. Elem.* **2013**, *37*, 187–196. [CrossRef]
23. Ku, C.Y. On solving three-dimensional Laplacian problems in a multiply connected domain using the multiple scale Trefftz method. *CMES Comput. Model. Eng. Sci.* **2014**, *98*, 509–541.
24. Ku, C.Y.; Liu, C.Y.; Xiao, J.E.; Yeih, W. Transient modeling of flow in unsaturated soils using a novel collocation meshless method. *Water* **2017**, *9*, 954. [CrossRef]
25. Li, P.W. The space–time generalized finite difference scheme for solving the nonlinear equal-width equation in the long-time simulation. *Appl. Math. Lett.* **2022**, *132*, 108181. [CrossRef]
26. Fang, J.; Al-Hamdan, M.Z.; O'Reilly, A.M.; Ozeren, Y.; Rigby, J.R.; Jia, Y. A novel floodwave response model for time-varying streambed conductivity using space-time collocation Trefftz method. *J. Hydrol.* **2023**, *625*, 129996. [CrossRef]
27. Li, P.W.; Hu, S.; Zhang, M. Numerical Solutions of the Nonlinear Dispersive Shallow Water Wave Equations Based on the Space-Time Coupled Generalized Finite Difference Scheme. *Appl. Sci.* **2023**, *13*, 8504. [CrossRef]
28. Langevin, C.D. Modeling axisymmetric flow and transport. *Groundwater* **2008**, *46*, 579–590. [CrossRef]

29. Theis, C.V. The relation between the lowering of the piezometric surface and the rate and duration of discharge of a well using ground-water storage. *Eos Trans. Am. Geophys. Union* **1935**, *16*, 519–524. [CrossRef]
30. Cheng, A.H.-D.; Ouazar, D. Theis solution under aquifer parameter uncertainty. *Groundwater* **1995**, *33*, 11–15. [CrossRef]